Graphene nanostructures as tunable storage media for molecular hydrogen

Serguei Patchkovskii[†], John S. Tse[†‡], Sergei N. Yurchenko[†], Lyuben Zhechkov[§], Thomas Heine[§], and Gotthard Seifert[§]

[†]Steacie Institute for Molecular Sciences, National Research Council Canada, 100 Sussex Drive, Ottawa, ON, Canada K1A 0R6; and [§]Institut für Physikalische Chemie und Elektrochemie, Technische Universität Dresden, D-01062 Dresden, Germany

Edited by James L. Dye, Michigan State University, East Lansing, MI, and approved June 2, 2005 (received for review February 9, 2005)

Many methods have been proposed for efficient storage of molecular hydrogen for fuel cell applications. However, despite intense research efforts, the twin U.S. Department of Energy goals of 6.5% mass ratio and 62 kg/m^3 volume density has not been achieved either experimentally or via theoretical simulations on reversible model systems. Carbon-based materials, such as carbon nanotubes, have always been regarded as the most attractive physisorption substrates for the storage of hydrogen. Theoretical studies on various model graphitic systems, however, failed to reach the elusive goal. Here, we show that insufficiently accurate carbon–H_2 interaction potentials, together with the neglect and incomplete treatment of the quantum effects in previous theoretical investigations, led to misleading conclusions for the absorption capacity. A proper account of the contribution of quantum effects to the free energy and the equilibrium constant for hydrogen adsorption suggest that the U.S. Department of Energy specification can be approached in a graphite-based physisorption system. The theoretical prediction can be realized by optimizing the structures of nano-graphite platelets (graphene), which are lightweight, cheap, chemically inert, and environmentally benign.

equilibrium constants | hydrogen storage | quantum effects

A recent report on hydrogen clathrate hydrate (1) shows that under high pressure, molecular hydrogen can be trapped in the clathrate cavities reaching a mass ratio close to that defined by the U.S. Department of Energy (DOE) (2). However, the hydrogen clathrate is only stable under high pressure or at very low temperature. Simple sterical considerations suggest that the use of a "help gas" to stabilize the clathrate hydrate under less severe thermodynamic conditions would lead to the deterioration of the hydrogen storage mass ratio and may not be viable for mobile applications. On the other hand, there have also been numerous experimental studies on the binding capacity of molecular hydrogen with graphitic substrates (3, 4). At technologically viable conditions, reliably reproducible results are still far from the DOE goal (3, 4). In the attempt to understand and improve the storage capacity of graphitic materials, calculations have been made on many models. Some of the calculations were based on empirical interaction potentials (5–9), and the others used potentials derived from quantum mechanical calculations (10–16). The role of quantum behavior of molecular hydrogen at low temperatures has also been investigated (6, 8, 17–19). Unfortunately, the binding capacity for hydrogen at near-ambient conditions has not been calculated, including the quantum effects and accurate, *ab initio*-based interaction potentials. To date, there has not been a reliable theoretical study indicating that the DOE goal of 6.5% mass ratio can or cannot be achieved in pure graphitic materials.

The interaction of nonpolar H_2 molecules with physisorption substrates in graphitic system is mainly the London dispersion. Accurate calculations including treatment of electron correlations on model systems, such as polycyclic aromatic hydrocarbons (PAHs) (e.g., benzene and coronene), indicate that H_2 molecules have adsorption energies between 4 and 7 kJ/mol (12, 14, 16) at an equilibrium distance of ≈3 Å. These binding energies are small and the entropic, and quantum effects cannot be ignored at practical temperatures (≈200–300 K). An adequate description of the motion of light H_2 molecule in the soft, anharmonic potential of a graphitic system is a prerequisite for accurate prediction of the equilibrium constant and, therefore, the binding capacity of molecular hydrogen in these systems (20). Although the thermodynamic behavior of the free H_2 gas in the 200- to 300-K temperature range is essentially classical, this is no longer true in the presence of soft external potentials. Quantum behavior of hydrogen adsorbed in narrow pores manifests itself in the quantum sieving effects (21), which persist up to 300 K (22). Inclusion of the quantum effects in the free energy is a nontrivial computational problem. It involves solving the Schrödinger equation for the motion of the hydrogen atoms on a complicated potential energy surface (PES).

Methods

A computationally tractable model of graphene is provided by quantum-mechanical description of H_2–PAH interactions with post-Hartree–Fock treatment of electron correlation (14, 16). We calculate the H_2–benzene PES using second-order Møller–Plessett (MP2) perturbation theory (16). Interaction energies and the PES shape in the H_2–benzene system are sensitive to the choice of the polarization functions and basis set superposition error (BSSE) (16). The BSSE in the interaction energy gradually decreases for larger basis sets, reaching just 0.6 kJ/mol for the aug-cc-pVQZ basis at the global minimum of the H_2/C_6H_6 PES (see Fig. 5, which is published as supporting information on the PNAS web site). The global minimum is found 4.95 kJ/mol below the separated H_2 and benzene. The counterpoise-corrected and uncorrected MP2/aug-cc-pVQZ equilibrium distances differ by only 0.04 Å.

By a fortuitous coincidence, BSSE-uncorrected MP2/cc-pVTZ results for the H_2–benzene model system closely mimic the counterpoise-corrected MP2/aug-cc-pVQZ calculations both at the global minimum and in the asymptotic region. Because MP2/cc-pVTZ calculations are significantly less expensive, this basis was used for the PES exploration in larger models (H_2–coronene below) and for test calculations with coupled-cluster treatment of the electron correlation.

In the global PES minimum, H_2 is aligned along the C_6 symmetry axis of benzene at 3.1 Å between the centres of mass of H_2 and C_6H_6. The energy profile shows a typical London-type $\approx r^{-6}$ long-range behavior (16) (Fig. 1). More sophisticated correlation treatment [CCSD(T)/cc-pVTZ] reduces the H_2–benzene interaction by 0.9 kJ/mol (14) (≈20%) compared with MP2/cc-pVTZ, whereas the geometry remains essentially unchanged.

Interaction of H_2 with larger PAHs of higher polarizabilities and smaller ionization potentials leads to stronger binding. For infinitely large graphene platelets, the interaction has been extrapolated to >7 kJ/mol at the MP2 level (16), whereas the intermolecular distance is unchanged with increase of the PAH size (12, 14, 16).

This paper was submitted directly (Track II) to the PNAS office.

Abbreviations: DOE, U.S. Department of Energy; DOS, density-of-states; LJ, Lennard–Jones; MP2, second-order Møller–Plessett; PAH, polycyclic aromatic hydrocarbon; PES, potential energy surface.

[‡]To whom correspondence should be addressed. E-mail: tse@ned.sims.nrc.ca.

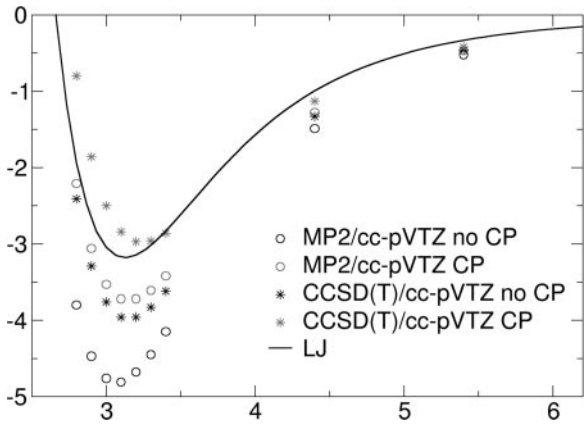

Fig. 1. H_2/benzene *ab initio* interaction potentials and fitted Lennard–Jones (LJ) potential. Potential energy E (in kJ/mol) is shown as a function of the distance of the centres of mass of H_2 and benzene (in Å). CP, results with the counterpoise correction applied.

The model system H_2/coronene considered here (Fig. 6 and Tables 3 and 4, which are published as supporting information on the PNAS web site) correctly reproduces the expected London-type r^{-6} long-range potential tail and only slightly underestimates the extrapolated H_2/graphene physisorption energy (16).

Direct *ab initio* evaluation of the sufficiently detailed PES of graphene would have been prohibitively expensive. Instead, we describe the H_2/graphene PES by the exp-6 form of the LJ pair potential $[v(r) = \Sigma_i(Ae^{-\alpha r_i} + C_6 r_i^{-6})]$, where r_i is the distance between H_2 centre of mass and carbon atom i. Parameters A, α, and C_6 are fitted to reproduce the MP2/cc-pVTZ results of the C_{6v}-symmetric H_2-coronene model system (Table 5, which is published as supporting information on the PNAS web site). The fitted LJ potential shows good agreement with *ab initio* results for the H_2–benzene system (Fig. 1; and see Figs. 6 and 7, which are published as supporting information on the PNAS web site). The fitted potential slightly underestimates (by 0.4 kJ/mol) the translational barriers between two adjacent minima (Fig. 6). This deviation is small compared with RT and is therefore not expected to affect thermodynamic properties. It is a good approximation to assume the H_2–PAH interaction energy to be additive and independent on the number of H_2 molecules interacting with the PAH (16).

For the evaluation of adsorption potential, we have chosen a two-dimensional, periodic graphite sheet with experimental C–C distance (R_{CC}). Contributions to the potential from 30 nearest primitive unit cells are included along the in-plane a and b directions. For the double-layer structures, the potential of two layers ("above" and "below" the H_2) is included. For short inter-layer separations, attraction due to the second-neighbor layer may further increase interaction energies. This effect was not considered in our simulations. The potential of the two-dimensionally periodic graphite layer is illustrated in Fig. 8, which is published as supporting information on the PNAS web site.

Free energies of adsorption were calculated in the ideal gas approximation

$$\Delta F = -RT\ln K_{\text{eq}} = -RT\ln\left(\frac{q_{\text{ads}}}{q_{\text{free}}}\right), \qquad [1]$$

where the canonical partition functions q_{ads} and q_{free},

$$q = \sum_i \exp\left(\frac{-\varepsilon_i}{kT}\right), \qquad [2]$$

are obtained from the energy levels ε_i, determined by solving the one-particle Schrödinger equation for H_2 motion in the adsorbing potential (q_{ads}) and in free space (q_{free}). Other thermodynamic functions (ΔE, ΔS, etc.) are obtained from ΔF, using standard expressions (23, 24).

All MP2 and CCSD(T) computations were performed with the NWCHEM (25) program package. Optimised B3LYP/6–31G* geometries were taken from previous work (16). Coordinates, corresponding energies, and further details on H_2/PAH computations are given in Tables 3, 4, and 6–8, which are published as supporting information on the PNAS web site.

The time-independent Schrödinger equation is solved for a single featureless particle with the mass of a hydrogen molecule. Calculations employ periodic boundary conditions and a plane wave basis set. To accelerate convergence of the free energies with the plane wave cutoff, identical unit cell dimensions and plane wave cutoffs are used for calculation of q_{ads} and q_{free}. The rectangular unit cell is obtained by replicating the primitive unit cell ($a_p = \sqrt{3}R_{CC}$, $b_p = 3R_{CC}$, $R_{CC} = 1.421$ Å) in a and b directions. To avoid the attractive artifacts of the exp-6 potential close to the nuclei and reduce the requirements for high-frequency basis set components, the simulation cell extent in the c direction was truncated by d_{excl} ($1.0 \le d_{\text{excl}} \le 2.0$ Å) in the vicinity of the graphene sheet(s). For double-layer structures with interlayer spacing d, the unit cell extent in the c direction is, therefore, $c = d - 2d_{\text{excl}}$. Single-layer simulations were performed by using the same periodic boundary conditions, but the interlayer spacing d was chosen to be large. The unit cell parameters, plane wave cutoffs, and calculated partition functions are given in Tables 9 and 10, which are published as supporting information on the PNAS web site.

We neglect contributions due to the adsorption-induced changes in the internal motion (rotation and vibration) of the H_2 molecules. The consequences of this approximation can be understood by using the PES of the H_2–benzene complex. Because of the stiffness of the H_2 molecule, only the change in the zero-point energy can contribute at temperatures of interest. At the C_{6v} minimum of the H_2–benzene PES, we calculate H_2 harmonic vibrational frequency of 4,494 cm^{-1}, 30 cm^{-1} below the free H_2 molecule. [Indeed, the softening of the H_2 vibrational mode appears to be a general trend upon physisorption of this molecule (26).] At 200 K, the (neglected) increase in the adsorption constant is $\exp(-\Delta v/2kT) - 1 \approx 11\%$, leading to a slight underestimation of the storage capacity.

The assessment of the rotational contribution to the partition function requires knowledge of the anisotropy of the adsorption potential. For the C_{6v} minimum of the H_2–benzene PES, the MP2/cc-pVTZ binding energy is -395 cm^{-1}. Binding energies of -261 cm^{-1} are found for the corresponding C_{2v}-symmetric structures with H_2 perpendicular to any of the benzene σ_v symmetry planes. Due to the large rotational level spacing of the H_2 molecule ($2B_e \approx 122$ cm^{-1}) and the effects of the nuclear spin statistics, the explicit treatment of the restricted rotation in this potential leads to a small (≈3%; see *Estimation of the Restricted Rotor Contribution to the H_2 Adsorption Free Energy* in *Supporting Text*, which is published as supporting information on the PNAS web site) increase in the adsorption constants, neglected in our calculations.

Dispersive interactions between the graphene layers were not explicitly considered in our simulations. This approach is equivalent to assuming that the layered host structure remains unchanged upon H_2 uptake. Because of the significant free energy cost associated with the graphene layer separation process (27), the "empty" layered structure must be stabilized by other means, such as spacers (see below).

Meaningful calculations of the free energy changes require that $K_{\text{eq}} = q_{\text{ads}}/q_{\text{free}}$ is converged with respect to the volume of the unit cell. From test calculations on the single-layer graphene structure, we find that unit cell $a = 3a_p$, $b = 2b_p$ leads to K_{eq} values converged to better than 15%. All calculations reported presently use these unit cell dimensions. Because tunneling of H_2 through the graphene

Table 1. Gravimetric and volumetric H_2 storage capacity of layered graphite structures

	p_{ext} = 5 MPa					p_{ext} = 10 MPa				
d, Å	p_{int}, MPa	w_{re}, %	w_{id}, %	v_{re}	v_{id}	p_{int}, MPa	w_{re}, %	w_{id}, %	v_{re}	v_{id}
				T = 300 K						
Free gas*				483	499				248	249
14	22	2.13	2.30	169	157	45	3.63	4.50	98	78
12	27	2.02	2.26	153	137	55	3.38	4.42	90	68
10	40	2.03	2.45	127	105	79	3.25	4.78	78	52
9	54	2.12	2.78	109	83	108	3.28	5.40	70	52
8	91	2.39	3.71	86	55	183	3.47	7.16	59	27
7	167	3.32	6.58	54	26	333	4.54	12.34	39	13
6	273	3.16	7.96	48	18	546	4.17	14.75	36	9
5.75	183	2.41	5.03	61	29	365	3.28	9.58	45	14
5.50	49	1.40	1.79	102	79	99	2.20	3.52	64	40
				T = 250 K						
Free gas*				387	416				201	208
14	34	3.49	4.10	102	86	68	5.45	7.88	64	43
12	43	3.30	4.12	93	73	85	5.02	7.92	60	37
10	65	3.26	4.68	78	54	129	4.73	8.94	53	27
9	93	3.36	5.56	68	40	186	4.69	10.53	48	20
8	175	3.69	8.13	55	24	349	4.88	15.04	41	12
7	397	5.11	16.74	34	9	794	6.43	29.68	27	5
6	784	4.89	22.95	31	5	1568	6.04	37.33	25	3
5.75	492	3.85	14.63	38	9	984	4.83	25.52	30	4
5.50	112	2.62	4.71	54	29	223	3.60	9.00	39	15

Parameter d is the interlayer distance. Quantities p_{ext} and p_{int} are, respectively, the external and internal H_2 pressure (see text), and w_{re} and w_{id} are weight fractions of H_2 in the material, estimated from the real (w_{re}) and ideal (w_{id}) gas equations of state. Corresponding apparent molar volumes (in cm^3/mol) are given by v_{re} and v_{id}.
*Weight fractions of H_2 in the free gas are 100%.

layer is associated with a very high barrier, we do not need to consider unit cells replication in the c direction.

The weak H_2–H_2 interaction is attractive at intermolecular distance >3.1 Å (28, 29). At higher hydrogen guest densities, H_2 can no longer be treated as an ideal gas. Although it is possible to simulate the high-density H_2/graphene system directly, using the grand canonical path integral Monte Carlo approach, such calculations are rather laborious and may be hard to interpret. At the same time, for slowly varying potentials adsorption free energy of an ideal gas is a good approximation to the adsorption free energy of the real gas *at the same number density* (see *Estimation of the Adsorption Free Energy of Nonideal H_2 Gas from the Results of an Ideal Gas Simulation and the Experimental Equation of State* in *Supporting Text* and refs. 23 and 24). We estimate the corrections due to H_2 nonideality at higher densities from an experimental equation of state (30) as follows: Given the external H_2 pressure p_{ext}, and the equilibrium constant K_{eq} obtained from the ideal gas simulation, we calculate the effective "internal" H_2 pressure p_{int} as

$$p_{int} = K_{eq} p_{ext}. \quad [3]$$

From p_{int} and the experimental H_2 equation of state (30), we obtain the molar volume v_{mol}. The apparent molar volume of H_2, characterizing volumetric efficiency of the storage system is then given by

$$v_{app} = \frac{d}{d - 2d_{excl}} v_{mol}. \quad [4]$$

For dual-layer system, the mass fraction of H_2 in the H_2/graphene system is given by

$$w = \frac{0.2633(d - 2d_{excl})}{v_{mol} + 0.2633(d - 2d_{excl})}, \quad [5]$$

where v_{mol} is in cm^3/mol and d, d_{excl} are in Å. The structural prefactor $3\sqrt{3}R_{CC}^2 N_A m_H/2{\cdot}10^{24} m_C \approx 0.2633$ cm^3/mol-Å is calculated from the fixed in-plane carbon–carbon distance R_{CC}, the atomic masses m_H and m_C of hydrogen and carbon, and the Avogadro constant N_A. Calculated internal pressure, volumetric and mass weight densities for representative temperatures, and external H_2 pressures are collected in Table 1 and Fig. 2.

The procedure outlined above is equivalent to treating graphene structure as a "nanopump," increasing the hydrogen pressure inside the structure, but otherwise leaving H_2 guest gas unaffected. Although approximate, this treatment allows us to completely sidestep the (still controversial) question of the choices H_2–H_2 interaction potentials, treatment of the quantum effects for H_2–H_2 interactions, and the associated convergence issues.

It is important to understand the approximations made in the nonideal gas estimation of the storage capacities v_{re} and w_{re}. Eq. **3** requires the use of fugacities f, rather than gas pressures p. As the f/p ratio decreases with pressure (at temperatures and pressures considered presently), Eq. **3** is expected to underestimate the internal pressure p_{int}. At the same time, using the free gas equation of state to calculate the molar volume neglects changes in H_2–H_2 radial distribution function due to the adsorption potential and, thus, overestimates the compressibility of the guest. Although these two defects may be expected to partially offset each other, the overall nonideality correction is at best semiquantitative. To illustrate the effect of the nonideality corrections, Table 1 also includes v_{id} and w_{id} values calculated from the ideal gas equation of state. When the real and ideal gas values are close, the residual error in the storage capacity is determined by the remaining uncertainties in the *ab initio* H_2/graphene interaction potential and the corresponding LJ fit. Based on the basis set and method convergence, we estimate this error at ±25% in v_{re} and w_{re}. When the real and ideal gas values deviate significantly from each other, the real gas result is clearly more reliable but should still be treated only as a semiquantitative estimate.

Results and Discussion

The spatial distribution of molecular hydrogen adsorbed on graphene is very delocalized (Fig. 3). This observation is in agreement with previous path-integral and Monte Carlo simulations (5, 15, 18)

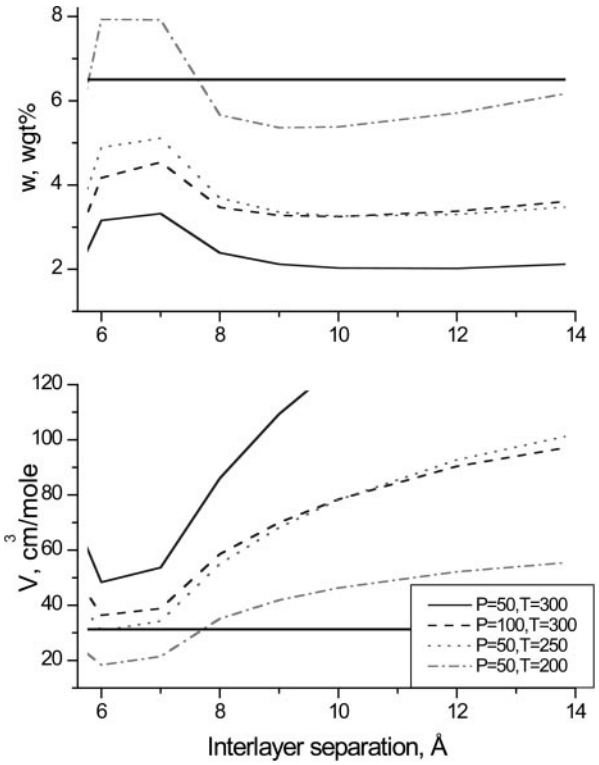

Fig. 2. Gravimetric (*Upper*) and volumetric (*Lower*) H_2 storage capacities of layered graphite structures, calculated from the real gas equation of state, as functions of the interlayer separation (see Table 1 and text). The DOE targets for automotive applications (2) ($w = 6.5\%$, $v = 31.2$ cm^3/mol) are indicated by solid horizontal lines.

and indicates an essentially free lateral motion of H_2. Our calculations indicate a slightly attractive (-1.2 kJ/mol) H_2-graphene free reaction energy at 300 K (see Table 2). The entropic contribution to the free energy is significant (ΔS_{300}). The physisorption free energy corresponds to an equilibrium constant of $K_{eq} = \exp(-\Delta F/RT) \approx 1.6$. In other words, at room temperature a single graphite layer increases the H_2 abundance by only ≈60%. The enhancement factor does not significantly change at lower temperatures (Fig. 4) or higher pressures. Considering the volume taken up by graphene itself, graphite surfaces are unsuitable for practical H_2 storage.

To improve the binding capacity, it is possible to sandwich H_2 between graphite layers. Binding energies of up to 30 kJ/mol have been reported for H_2 inside carbon nanotube tips (11). We have calculated quantum-mechanical physisorption free energies for interlayer distances d, between two graphite layers ranging from 4 to 14 Å. As can be seen from the results in Table 2, at separations above 7 Å the zero-temperature enthalpy of the H_2–graphite interaction is very similar for bi- and monolayer structures (12). Even at these separations, the free energy is strongly affected by the presence and position of the second layer (Table 2 and Fig. 4). We predict an increase in H_2 binding free energy with decreasing layer separation up to a maximum of ≈10 kJ/mol for an interlayer distance of ≈6 Å. For smaller separations, exchange repulsion reduces the free energy considerably (Fig. 4), which becomes positive for interlayer separations <5 Å. The thermodynamics of the H_2/graphite system at shorter separations is purely repulsive (31). The calculated equilibrium constant shows a sharp "peak" at 6–7 Å (Fig. 2 *Upper*). Consequently, experimental fine-tuning of K_{eq} should be taken with care; too small a separation could readily lead to a collapse in the adsorption free energy. At ambient conditions ($T = 298$ K, $P = 0.1$ MPa), we estimate maximum equilibrium constant of ≈30, for a graphite–graphite interlayer distance of 7 Å.

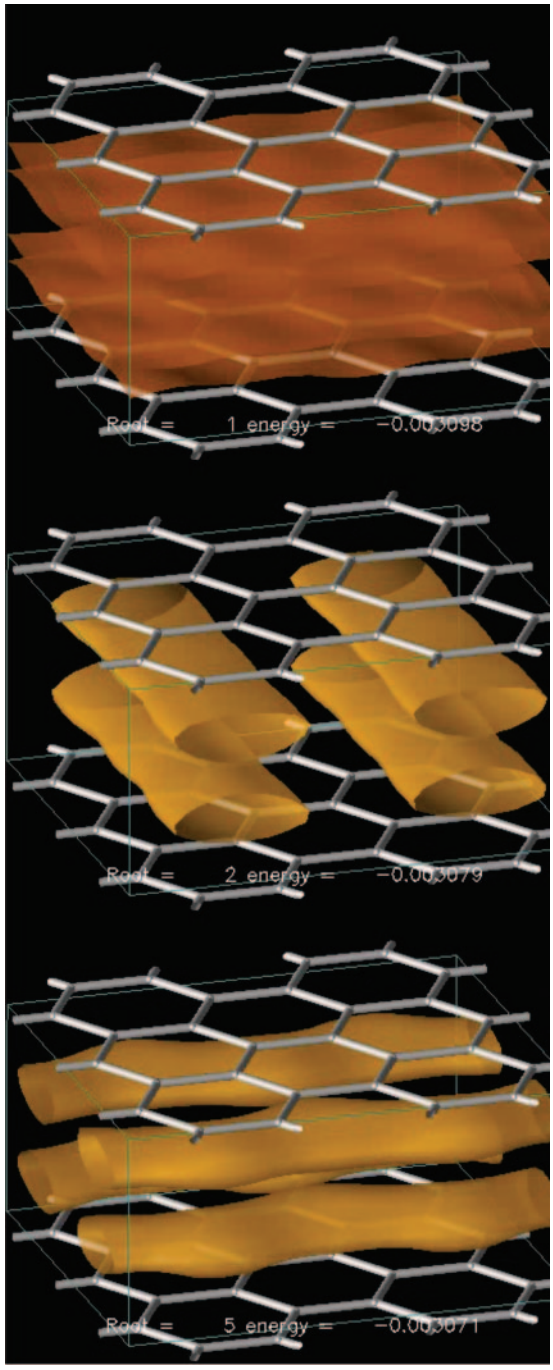

Fig. 3. Probability densities for selected lowest eigenstates of the translational nuclear Hamiltonian. The lowest in-phase (*Top* to *Bottom*: first, second, and fifth) eigenstates for the double-layer structure are shown ($d = 8$ Å).

The very favorable adsorption free energies for $d = 6$–7 Å effectively creates a "nanopump," increasing the internal H_2 pressure inside the layered structure (see Table 1). As a result, the target of 62 kg/m^3 (≈31 cm^3/mol) volumetric storage density, set by the DOE, can be approached at a moderate external H_2 pressure (≈10 MPa) even at room temperature.

At the same time, our simulations indicate that a pure carbon-based storage system cannot achieve the DOE gravimetric storage target (6.5 wt % H_2) at room temperature and moderate pressures. Due to the increasingly nonideal behavior of H_2 at high internal pressures, room-temperature storage capacity is limited to 2–3 wt

Table 2. Free energy of H_2 adsorption on graphite surfaces and in graphite layered structures

d, Å	ΔE_0,* kJ/mol	ΔF_{300}, kJ/mol	ΔE_{300}, kJ/mol	ΔS_{300}, J/mol-K	K_{300}
∞†	−6.2	−1.2	−2.4	−4.0	1.6
12.0	−6.4	−4.2	−5.3	−3.7	5.5
10.0	−6.7	−5.2	−6.0	−2.9	7.9
9.0	−7.1	−5.9	−6.7	−2.5	10.8
8.0	−8.1	−7.2	−8.1	−2.7	18.3
7.0	−11.0	−8.7	−10.8	−6.7	33.3
6.0‡	−13.0	−10.0	−13.1	−10.4	54.6
5.5‡	−10.1	−5.7	−10.1	−14.7	9.9
5.0‡	+1.2	+7.2	+1.7	−18.2	0.06

Results for quantum computations of ideal-gas H_2 in external graphite potentials. Parameter d is the interlayer distance. $\Delta F_0 = \Delta E_0$ and ΔF_{300} are free energies of H_2 adsorption at 0 K and 300 K, respectively. The energy and the enthropy of adsorption at 300 K are given by ΔE_{300} and ΔS_{300}, and K_{300} is the equilibrium constant.
*H_2 ground state energy in the adsorbing potential.
†The infinite distance is computed in a box with interlayer spacing $d = 43$ Å.
‡Values at these interlayer separations may be affected by the shape of the repulsive part of the potential, leading to an increase in the error bars.

% at 5 MPa, and 3–4 wt % at 10 MPa. Although not yet achieving the DOE target, this storage capacity is already competitive with best known physisorption substrates. We calculated similar room-temperature gravimetric storage capacities for a wide range of interlayer spacing (d = 7–12 Å; see Fig. 2), which should simplify practical design of the storage material.

Lower but still technologically acceptable temperatures can increase the equilibrium constant by at least one order of magnitude. Fig. 4 illustrates the temperature dependence of the equilibrium constants for a bilayer with $d = 8$ Å. Although our treatment of H_2–H_2 interactions becomes increasingly uncertain at lower temperatures (see *Methods*), the simulations indicate that gravimetric storage capacities of 5.0–6.5 wt % of H_2 should be achievable at technologically acceptable conditions, e.g., at $T = 250$ K, $P_{ext} = 10$ MPa or $T = 200$ K, $P_{ext} = 5$ MPa (Table 1 and Fig. 2). Because these storage capacities are only weakly sensitive to the graphite interlayer separation, the design of the necessary layered graphite structure does not appear to be an insurmountable challenge.

Caution should be applied in interpreting the results of our simulations for small interlayer distances ($d \leq 9$ Å). At low pressures, van der Waals close-packing arguments suggest that at most two H_2 monolayers (6.6 wt %) can fit between the graphene layers separated by $d = 9$ Å. For $d = 6$ Å, just one monolayer can fit in the structure, indicating a maximum H_2 storage capacity of 3.3 wt % (3, 4). Although this argument holds at low pressures, the large adsorption free energy calculated for small interlayer spacing can drive the internal pressure beyond 2 kbar (1 bar = 100 kPa), even at moderate external pressures (Table 1). In the free hydrogen gas, the density at such pressures exceeds the close-packing limit (30). At the same time, our approach to H_2–H_2 interactions is crude, so that the pronounced maximum in H_2 storage capacity we find at interlayer spacing 6 Å $\leq d \leq$ 7.5 Å should be considered only as a

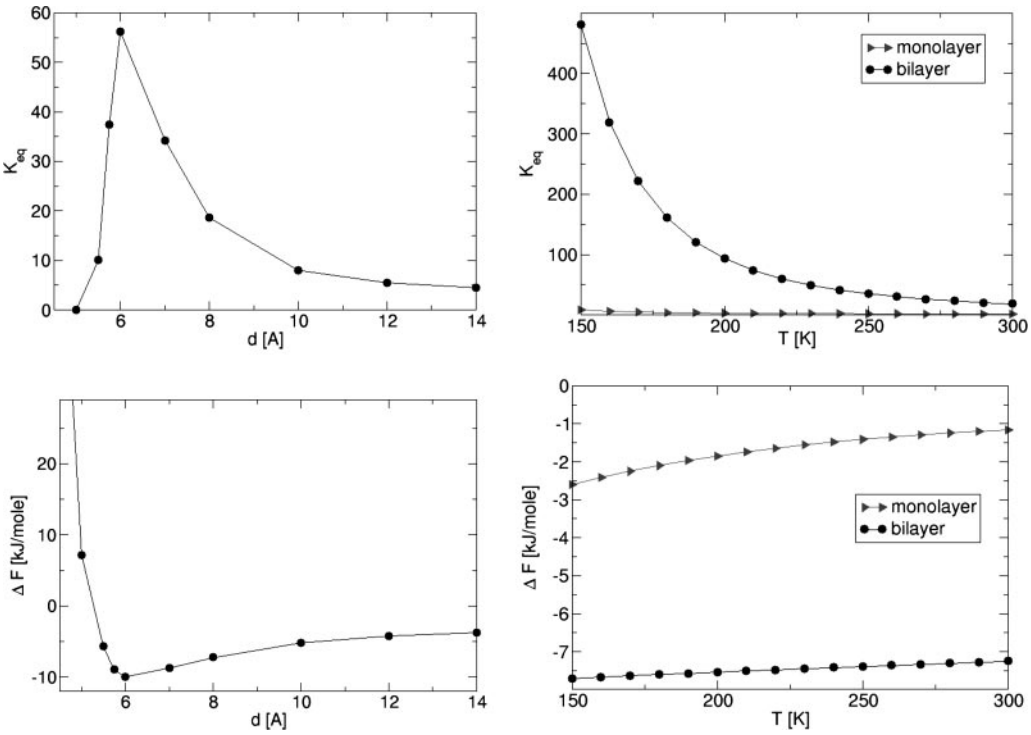

Fig. 4. Equilibrium constants K_{eq} (*Upper*) and reaction free energies ΔF (*Lower*; in kJ/mol) are plotted as a function of the interlayer distance d (*Left*; in Å, at $T = 300$ K) and temperature T (*Right*; in K, at $d = 8$ Å), respectively.

tantalizing possibility. Confirming or disproving its existence would require further, more elaborate simulations (or experiment).

The qualitative difference in the H_2 storage capacity of mono- and bilayer graphite is easily understood by comparing the density-of-states (DOS) (Fig. 9, which is published as supporting information on the PNAS web site) for the two models. The single-layer graphite potential creates relatively few H_2 bound states, which are localized at the graphite surface. For the majority of states, the DOS is very similar to the DOS of free H_2, reflecting the short-range nature of the binding potential. For the double-layer structure, DOS has many binding states, with the bulk of the available states shifted to low energies. In other words, whereas free H_2 can move away from a single layer and hence on average experiences little attraction, H_2 inside a double-layer structure is always in an attractive potential. Fig. 3 shows probability densities of H_2 in between two graphite layers, for a few lowest states. Even low-energy modes are delocalized on the surface. The abundance of low-energy surface modes on graphite and in sandwiched structures suggests the presence of a two-dimensional H_2 gas. The lateral modes should facilitate diffusion inside the storage material, thus ensuring easy loading and unloading.

The estimated limit of accuracy of our calculations at $d \geq 8$ Å is within $\pm 25\%$ (see *Methods*). Even considering this large margin of error, we conclude that an H_2 storage enhancement material approaching, or possibly even exceeding, the DOE specification can be produced by encapsulating molecular hydrogen in graphite layers with an appropriate interlayer spacing. The significant dependence of the equilibrium constant on the graphite interlayer distance indicates that the H_2 abundance of a nanostructured graphite system is intimately controlled by the nano- and mesoscopic structure. Together with the pronounced temperature dependency, the controversial issue of the qualitatively different amounts of H_2 adsorption in the literature of the last decade (5, 10, 32–34) on graphite systems may well arise from slight microstructural variations both within and between different samples.

It is hence an experimental challenge to provide a synthesis of nanostructured graphite with sufficiently uniform and reproducible interlayer distances suitable for H_2 storage. One possibility is to introduce well defined spacers. Aside from the tuning possibilities, the spacers may provide additional benefits, such as an increase in the stability of the storage media. Spacers can also act as molecular sieves, preventing penetration of larger gas molecules such as N_2, CO, and CO_2, which typically have a higher graphene binding energy than H_2 and may reduce storage capacity (21). For example, we compute the binding energy of the N_2/benzene model system to be two times larger than the comparable H_2/benzene model.

One possibility for the experimental realization of the layered graphene storage system is provided by graphite intercalation compounds, which exhibit a wide range of interlayer separations (35). Achieving the optimal H_2 storage capacity requires a stage-1 intercalation compound, with guest molecules appearing after each graphene sheet. Stable stage-1 species with interlayer separations from 3.7 to 12 Å are known (35), offering almost unlimited possibilities for chemical tuning. One of the experimental challenges in synthesizing our storage system lies in minimizing the interlayer volume, excluded by the spacers. This goal can be achieved by preparing a mixed intercalation compound with two guests of a different size. The larger guest can be chemically or photochemically cross-linked to the graphene host, followed by elimination of the weakly bound smaller guest. Chemical cross-linking may partially disrupt the graphene π-system, somewhat decreasing the van der Waals interactions and the adsorption free energy. At the same time, sufficiently polar spacers can increase electrostatic interactions enough to more than compensate for this loss (15).

Another prototype for the storage system is carbon foam (36) with the structure based on rigidly interconnected segments of graphite. In principle, the interlayer separation can be adjusted by extending the interlayer carbon skeleton. The resulting "foam" structures cover the structural phase space extending from hexagonal diamond to graphite. A previous theoretical study (36) has shown that this hybrid system possesses unusually high structural stability and low mass density.

S.P. thanks Dr. D. D. Klug for helpful discussions. This work was supported by the Deutsche Forschungsgemeinschaft, the Stiftung Energieforschung Baden-Württemberg, and the National Sciences and Engineering Research Council of Canada.

1. Mao, W. L., Mao, H.-K., Goncharov, A. F., Struzhkin, V. V., Guo, Q., Hu, J., Shu, J., Hemley, R. J., Somayazulu, M. & Zhao, Y. (2002) *Science* **297,** 2247–2249.
2. Schlapbach, L. & Zuttel, A. (2001) *Nature* **414,** 353–358.
3. Hirscher, M., Becher, M., Haluska, M., von Zeppelin, F., Chen, X., Dettlaff-Weglikowska, U. & Roth, S. (2003) *J. Alloys Compd.* **356,** 433–437.
4. Züttel, A., Wenger, P., Sudan, P., Mauron, P. & Orimo, S. (2004) *Mater. Sci. Eng. B* **108,** 9–18.
5. Darkrim, F., Vermesse, J., Malbrunot, P. & Levesque, D. (1999) *J. Chem. Phys.* **110,** 4020–4027.
6. Hathorn, B. C., Sumpter, B. G. & Noid, D. W. (2001) *Phys. Rev. A* **64,** 022903.
7. Cracknell, R. F. (2002) *Mol. Phys.* **100,** 2079–2086.
8. Lu, T., Goldfield, E. M. & Gray, S. K. (2003) *J. Phys. Chem. B* **107,** 12989–12995.
9. Piseri, P., Barborini, E., Marino, M., Milani, P., Lenardi, C., Zoppi, L. & Colombo, L. (2004) *J. Phys. Chem. B* **108,** 5157–5160.
10. Arellano, J. S., Molina, L. M., Rubio, A. & Alonso, J. A. (2000) *J. Chem. Phys.* **112,** 8114–8119.
11. Okamoto, Y. & Miyamoto, Y. (2001) *J. Phys. Chem. B* **105,** 3470–3474.
12. Tran, F., Weber, J., Wesolowski, T. A., Cheikh, F., Ellinger, Y. & Pauzat, F. (2002) *J. Phys. Chem. B* **106,** 8689–8696.
13. Zhang, X., Cao, D. & Chen, J. (2003) *J. Phys. Chem. B* **107,** 4942–4950.
14. Hübner, O., Glöss, A., Fichtner, M. & Klopper, W. J. (2004) *Phys. Chem. A* **108,** 3019–3023.
15. Deng, W.-Q., Xu, X. & Goddard, W. A. (2004) *Phys. Rev. Lett.* **92,** 1666103.
16. Heine, T., Zhechkov, L. & Seifert, G. (2004) *Phys. Chem. Chem. Phys.* **6,** 980–984.
17. Wang, Q. U., Johnson, J. K. & Broughton, J. Q. (1996) *Mol. Phys.* **89,** 1105–1119.
18. Wang, Q. Y. & Johnson, J. K. (1998) *Mol. Phys.* **95,** 299–309.
19. Gu, C. & Gao, G.-H. (2002) *Phys. Chem. Chem. Phys.* **4,** 4700–4708.
20. Patchkovskii, S. & Yurchenko, S. N. (2004) *Phys. Chem. Chem. Phys.* **6,** 4152–4155.
21. Wang, Q., Challa, S. R., Sholl, D. S. & Johnson, J. K. (1999) *Phys. Rev. Lett.* **82,** 956–959.
22. Trasca, R. A., Kostov, M. K. & Cole, M. W. (2003) *Phys. Rev. B* **67,** 035410.
23. Hill, T. L. (1986) *An Introduction to Statistical Thermodynamics* (Dover, New York).
24. Hill, T. L. (1987) *Statistical Mechanics* (Dover, New York).
25. Straatsma, T. P., Apra, E., Windus, T. L., Bylaska, E. J., de Jong, W., Hirata, S., Valiev, M., Hackler, M. T., Pollack, L., Harrison, R. J., *et al.* (2005) NWCHEM (Pacific Northwest National Laboratory, Richland, WA), Version 4.7.
26. Patchkovskii, S. & Tse, J. S. (2003) *Proc. Natl. Acad. Sci. USA* **100,** 14645–14650.
27. Girifalco, L. A. & Lad, R. A. (1956) *J. Chem. Phys.* **25,** 693–697.
28. Diep, P. & Johnson, J. K. (2000) *J. Chem. Phys.* **113,** 3480–3481.
29. Diep, P. & Johnson, J. K. (2000) *J. Chem. Phys.* **112,** 4465–4473.
30. Mills, R. L., Liebenberg, D. H., Bronson, J. C. & Schmidt, L. C. (1977) *J. Chem. Phys.* **66,** 3076–3084.
31. Chan, S. P., Ji, M., Gong, X. G. & Liu, Z. F. (2004) *Phys. Rev. B* **69,** 092101.
32. Hirscher, M., Becher, M., Haluska, M., Dettlaff-Weglikowska, U., Quintel, A., Duesberg, G. S., Choi, Y.-M., Downes, P., Hulman, M., Roth, S., *et al.* (2001) *Appl. Phys. Mater. Sci. Proc.* **72,** 129–132.
33. Hirscher, M., Becher, M., Haluska, M., Quintel, A., Skakalova, V., Choi, Y.-M., Dettlaff-Weglikowska, U., Roth, S., Stepanek, I., Bernier, P., *et al.* (2002) *J. Alloys Compd.* **330,** 654–658.
34. Chambers, A., Park, C., Baker, R. T. K. & Rodriguez, N. M. (1998) *J. Phys. Chem. B* **102,** 4253–4256.
35. Enoki, T., Suzuki, M. & Endo, M. (2003) *Graphite Intercalation Compounds and Applications* (Oxford Univ. Press, Oxford).
36. Umemoto, K., Saito, S., Berber, S. & Tomanek, D. (2001) *Phys. Rev. B* **64,** 193409.